Hindawi
Journal of Chemistry
Volume 2019, Article ID 4329609, 11 pages
https://doi.org/10.1155/2019/4329609

Research Article

Preparation of Pore-Size Controllable Activated Carbon from Rice Husk Using Dual Activating Agent and Its Application in Supercapacitor

Khu Le Van and Thuy Luong Thi Thu

Faculty of Chemistry, Hanoi National University of Education, Hanoi 1000, Vietnam

Correspondence should be addressed to Khu Le Van; khulv@hnue.edu.vn

Received 17 August 2018; Revised 27 November 2018; Accepted 6 December 2018; Published 15 January 2019

Guest Editor: Gassan Hodaifa

Copyright © 2019 Khu Le Van and Thuy Luong Thi Thu. This is an open access article distributed under the Creative Commons Attribution License, which permits unrestricted use, distribution, and reproduction in any medium, provided the original work is properly cited.

Activated carbons prepared from rice husk by chemical activation with dual activation agents, KOH and NaOH, have been studied and characterized by BET, SEM, EDX, FTIR, Boehm titration, Raman, and TGA. It was found that the KOH/NaOH impregnation ratio plays an important role on textural properties of AC. At the same amount of total alkali hydroxide, the KOH/NaOH ratio higher than 1.33 resulted in larger specific surface area (2990~3043 $m^2 \cdot g^{-1}$), microporous surface area (2747~2831 $m^2 \cdot g^{-1}$), and higher micropore volume (1.4250~1.4316 $cm^3 \cdot g^{-1}$). The as-prepared samples exist in the form of spherical-shaped particles with the size ranging from 20 to 60 nm and contain numerous surface functional groups. The as-prepared activated carbons were then assessed as an electrode material of supercapacitor operating in the 0.5 M K_2SO_4 electrolyte in potential windows of −1.0~0.0 V. The highest capacitance obtained was 205 $F \cdot g^{-1}$ at the scan rate of 2 $mV \cdot s^{-1}$ and 225 $F \cdot g^{-1}$ at a current density of 0.2 $A \cdot g^{-1}$. At the scan rate as high as 50 $mV \cdot s^{-1}$, all the as-prepared activated carbons in this study have the specific capacitance greater than 100 $F \cdot g^{-1}$.

1. Introduction

It is well known that activated carbon (AC) is a material with a porous structure and high specific surface area and is widely used as an adsorbent in water/air treatment, catalyst supporter, or electrical energy/gas storage material. By utilizing agricultural wastes, the synthesis of AC becomes more cost-effective which helps us to speed up the commercialization process measurably.

The preparation of AC consists of two stages: the carbonization stage at lower temperature and the activation stage at elevated temperature. Due to the advantage of lower temperature, shorter time, and developed porous structure, chemical activation is usually chosen over physical activation. In the chemical activation process, the chars (carbonized materials) are impregnated in activation agents such as potassium hydroxide (KOH), sodium hydroxide (NaOH), zinc chloride ($ZnCl_2$), and phosphoric acid (H_3PO_4) followed by activation at temperature in the range between 600 and 900°C under nitrogen flow. The characteristics of the resulting AC are very sensitive to preparing conditions, especially types of activating agents. The activated carbons prepared from lapsi seed (Nepal) are highly porous when activated by KOH or $CaCl_2$ than nonactivating agent pyrolyzed char; on the other hand, the activated carbons impregnated with $MgCl_2$, $FeCl_3$, and H_2SO_4 do not show porous structure [1]. Activated carbons prepared from macadamia nutshells have more microporous structure when activated by KOH while have more mesoporous structure when activated by $ZnCl_2$ [2]. With agricultural waste precursors, the alkali hydroxide activating agent produces more developed surface area than other salts, oxides, or acids. For example, *Enteromorpha prolifera* (China) based activated carbon activated by KOH resulted in higher surface area and larger total pore volume than that activated by $H_4P_2O_7$ [3]; tomato paste processing industry waste (Turkey) established highest surface area that was activated by KOH, much larger than by K_2CO_3 or HCl [4].

Furthermore, for rice husk, because of its high silica content, alkali hydroxide leaching is a preferable method for AC preparation. Comparative researches between KOH and NaOH have been conducted and showed that NaOH activation can satisfactorily control the mesopore volume of the activated carbons [5]. The KOH ACs had higher micropore volumes, whereas NaOH ACs had relatively higher densities [6]. Another difference between the activation process by KOH and NaOH is that KOH can be used effectively with any types of materials while NaOH only with disorder materials. This is ascribed to the intercalating ability of metallic K compared to metallic Na produced during the redox reactions. Metallic Na can only intercalate into the highly disorganized materials [7]. Nevertheless, no study has been conducted to use both KOH and NaOH as well as the effect of the KOH/NaOH ratio on the properties of activated carbon.

The main objective of this work is to prepare AC from rice husk with high porosity and large specific surface area using dual activating agent (KOH and NaOH) and investigate the effect of the NaOH/KOH ratio on the specific surface area, pore structure, morphology, and thermal stability of the AC samples. Moreover, the obtained materials were characterized and evaluated for potential application as supercapacitor electrode materials.

2. Materials and Methods

2.1. Materials and Chemicals. Rice husk was collected from Vinh Phuc Province, Vietnam. The raw precursor was washed, oven-dried at 110°C for 12 h, grounded, and then sieved to obtain uniform particle with a diameter of 1.0 mm. All chemicals used were of analytical reagent grade, and distilled water was used to prepare all solutions.

2.2. Preparation of Activated Carbon. The prepared husks were first carbonized at 500°C for 90 min in nitrogen atmosphere. The resulting chars were then impregnated with KOH and NaOH under various impregnation weight ratios as indicated in Table 1. For comparison, the chars were also impregnated with only KOH or NaOH (with the same molar ratio). The activation process was carried out in a tube furnace under nitrogen flow of 300 mL·min^{-1} and at heating rate of 10°C·min^{-1}. The samples were heated to 400°C and left for 20 min, and then afterwards, the temperature was raised to 850°C and maintained for 90 min (following our previous research [8] and other literatures [9]). The activated products were washed sequentially with 0.1 M HCl solution and hot distilled water to the neutral pH range (6.6–7.0). Finally, the activated carbon samples were dried at 120°C for 24 h and stored for use. The as-prepared samples were labeled as presented in Table 1.

2.3. Characterization of Activated Carbons. Textural properties of the ACs were measured from N_2 adsorption/desorption isotherms at 77 K (Micromeritics, TriStar 3020). The specific surface area (S_{BET}) was calculated by the Brunauer–Emmet–Teller (BET) equation [10]; the microporous surface area (S_{mic}), external surface area (S_{ext}), and micropore volume (V_{mic}) were evaluated by the *t*-plot method [11]; and the mesopore volume (V_{mes}) was obtained by the Barrett–Joyner–Halenda (BJH) method [12]. The total pore volume (V_{tot}) was evaluated by the sum of microporous and mesoporous volumes. The pore-size distribution of AC samples was calculated using density functional theory (DFT) [13] with the assumption that the pores of the sample have slit shape.

Table 1: AC samples prepared under various impregnation ratios.

Sample	Impregnation ratio KOH : NaOH : char (wt. ratio)
RH-K4N0	4 : 0 :1
RH-K0N3	0 : 3 : 1
RH-K1N2	1 : 2 : 1
RH-K1.5N2	1.5 : 2 : 1
RH-K2N2	2 : 2 : 1
RH-K2N1.5	2 : 1.5 : 1
RH-K2N1	2 : 1 : 1

The morphology of the activated carbons was observed using a field-emission scanning electron microscope S4800 (Hitachi). The element analysis was determined using SM-6510LV (Jeol).

The surface chemistry characteristics were identified by Fourier-transform infrared spectroscopy (Nicolet, Nexus 670) operating in a wave number range of 500–4000 cm^{-1} and employing the potassium bromide pellet method.

The concentrations of surface acidic/basic functional groups were determined by following the Boehm titration method [14] and were calculated under the assumption that NaOH neutralizes carboxylic, phenolic, and lactonic groups; Na_2CO_3 neutralizes both carboxylic and lactonic groups; and $NaHCO_3$ neutralizes only carboxylic groups. The amount of basic groups was calculated from the amount of hydrochloric acid consumed by the ACs.

Raman spectra were obtained with the Renishaw Raman microscope using an excitation wavelength at 250 nm.

The thermal behavior was performed with the thermogravimetric analyzer (DTG-60H, Shimazu). Before measurement, the AC samples were dried in air at 120°C in 2 h to remove adsorbed water. Then, the AC samples were heated from 120 to 650°C in pure air (flow rate 50 mL·min^{-1}) at a ramping rate of 10°C min^{-1}. Measurements were made using calcined alumina as reference material.

2.4. Electrode Preparation and Electrochemical Measurement. A mixture of activated carbon, conductive additive (carbon black), and binder (polytetrafluoroethylene) with weight ratio 8 : 1 : 1 was dispersed in ethanol. The slurry was laminated on each side of the current collector (nickel foam) and dried in oven at 120°C for 15 h. The resulting electrode was then pressed under 20 MPa and cut into 1 cm × 1 cm geometry shape. Electrochemical measurements were conducted in a three-electrode cell using an Autolab 302N instrument. The as-prepared activated carbon electrode was used as the working electrode, with saturated calomel

electrode (SCE) as the reference electrode, platinum sheet as the counterelectrode, and 0.5 M K_2SO_4 as well as 0.5 M Na_2SO_4 aqueous solutions as the neutral electrolytes. Cyclic voltammetry (CV) measurements were performed with a potential window from −1.0 to 0.0 V vs. SCE at scan rates from 2 to 100 mV·s^{-1}. Galvanostatic charge/discharge was carried out with the same potential window at current densities from 500 to 2000 mA·g^{-1}.

Specific capacitance based on CV measurements was calculated by the following equation:

$$C_{CV} = \frac{\sum |I| \Delta t}{2m\Delta V}, \quad (1)$$

while the gravimetric specific capacitance based on charge/discharge curves was evaluated by the following equation:

$$C_{CP} = \frac{I_d \Delta t_d}{m\Delta V}, \quad (2)$$

where $\sum |I| \Delta t$ is the area of the current (A) against the time (s) curve, m is the mass of the active material in the electrode (g), I_d is the discharge current (A), Δt_d is the discharge time (s), and ΔV is the potential interval (V).

3. Results and Discussion

3.1. Activated Carbon Characterization

3.1.1. Porous Texture. Nitrogen adsorption/desorption isotherms at 77K of AC samples prepared at different KOH/NaOH impregnation ratios are shown in Figure 1. All the isotherms are a combination of type I at low relative pressures (p/p°) and type IV at intermediate and high relative pressures according to IUPAC classification [15] with hysteresis loops, indicating the coexistence of micropores and mesopores.

Physical properties of AC samples obtained from N_2 adsorption isotherms are summarized in Table 2. It can be observed that the samples activated with single activation agent, RH-K4N0 and RH-K0N3, have different pore structures despite having the same amount of alkaline molecules. RH-K4N0 has higher specific surface area (2696 $m^2 \cdot g^{-1}$) consisting mainly of micropores while RH-K0N3 is detected with about 20% percent of mesopores (0.4396 $cm^3 \cdot g^{-1}$). This result is in good agreement with other research studies [16]. Nevertheless, the BET surface of single agent activated samples is smaller than that of all the samples activated with dual activation agents (S_{BET} is in the range of 2365~3043 $m^2 \cdot g^{-1}$). Therefore, it could be deduced that using dual activation agents enhances the development of the surface area of the activated carbon.

The effect of employing the dual activation agent KOH and NaOH on porous characteristic of the obtained activated carbon can also be seen from Table 2. The specific surface areas and the total pore volume were lowest when the alkali hydroxide/char impregnation ratio is 3.0 (2365 $m^2 \cdot g^{-1}$ and 1.2002 $cm^3 \cdot g^{-1}$ for RH-K1N2; 2829 $m^2 \cdot g^{-1}$ and 1.3636 $cm^3 \cdot g^{-1}$ for RH-K2N1). When the alkali hydroxide/char impregnation ratio is higher than 3.0, specific surface area and total pore volume increased to a certain degree (2945~3043 $m^2 \cdot g^{-1}$ and 1.7212~1.8084 $cm^3 \cdot g^{-1}$, respectively), which indicate that surface pyrolysis and interior etching processes happened concurrently.

While the amount of impregnated alkali hydroxide tends to affect the pore texture of the AC samples, the KOH/NaOH ratio however seems to have more influence. The S_{BET} was significantly increased from 2365 to 3043 $m^2 \cdot g^{-1}$ at KOH/NaOH ratios from 0.50 to 1.33. Nevertheless, as the KOH/NaOH ratio further increased to 2.00, S_{BET} decreased to 2990 $m^2 \cdot g^{-1}$. Additionally, the following points were observed from Table 2:

(i) At the same amount of alkali hydroxide, higher KOH content gave larger specific surface area, microporous surface area, and higher micropore volume. RH-K1N2 has S_{BET} = 2365 $m^2 \cdot g^{-1}$, S_{mic} = 2258 $m^2 \cdot g^{-1}$, and V_{mic} = 1.0156 $cm^3 \cdot g^{-1}$, while RH-K2N1, at the same amount of alkali hydroxide (alkali hydroxide/char = 3.0), led to S_{BET} = 2829 $m^2 \cdot g^{-1}$, S_{mic} = 2736 $m^2 \cdot g^{-1}$, and V_{mic} = 1.2267 $cm^3 \cdot g^{-1}$. The same situation happened with RH-K1.5N2 and RH-K2N1.5 (alkali hydroxide/char = 3.5), and S_{BET}, S_{mic}, and V_{mic} of RH-K1.5N2 (2945, 2745 $m^2 \cdot g^{-1}$, and 1.3811 $cm^3 \cdot g^{-1}$) are always lower than that of RH-K2N1.5 (3043, 2831 $m^2 \cdot g^{-1}$, and 1.4250 $cm^3 \cdot g^{-1}$).

(ii) At the same amount of the KOH/char ratio, as the NaOH/char ratio increased from 1.0 to 1.5 (RH-K2N1 and RH-K2N1.5), specific surface area and micropore surface area increased from 2829 and 2736 $m^2 \cdot g^{-1}$ to 3043 and 2831 $m^2 \cdot g^{-1}$. When the NaOH ratio further increased to 2.0 (RH-K2N2), specific surface area and micropore surface area decreased slightly to 2990 and 2747 $m^2 \cdot g^{-1}$. However, external surface area, mesopore volume, and total pore volume increased with the increase of the NaOH ratio from 1 to 2 (S_{ext}, V_{mes}, and V_{tot} increase from 93 $m^2 \cdot g^{-1}$, 0.1369, and 1.3636 $cm^3 \cdot g^{-1}$ to 243 $m^2 \cdot g^{-1}$, 0.3768, and 1.8084 $cm^3 \cdot g^{-1}$, respectively).

(iii) At the same amount of the NaOH/char ratio, when the KOH/char ratio increased gradually from 1 (RH-K1N2) to 1.5 (RH-K2N1.5) and 2 (RH-K2N2), specific surface area as well as total pore volume increased, reaching the highest value of 2990 $m^2 \cdot g^{-1}$ and 1.8084 $cm^3 \cdot g^{-1}$. This raise is resulted from the increase of micropore and mesopore, which were from 2258 and 107 $m^2 \cdot g^{-1}$ to 2747 and 243 $m^2 \cdot g^{-1}$.

The change in specific surface area and pore characteristic of AC samples with KOH/char and NaOH/char ratios might be explained by the formation of alkali metal through the reaction of hydroxide and carbon in the process of preparation of AC [17, 18] and by the lower boiling point of KOH (758°C) than NaOH (883°C [19]). It is easier for potassium to diffuse into the layer of carbon, causing the enhancement of pores (especially micropore), which in turn increases the specific and microporous surface area as well as the microporous volume of AC samples. As a result, the variation of Na content only causes the change in external site and mesopore of AC samples.

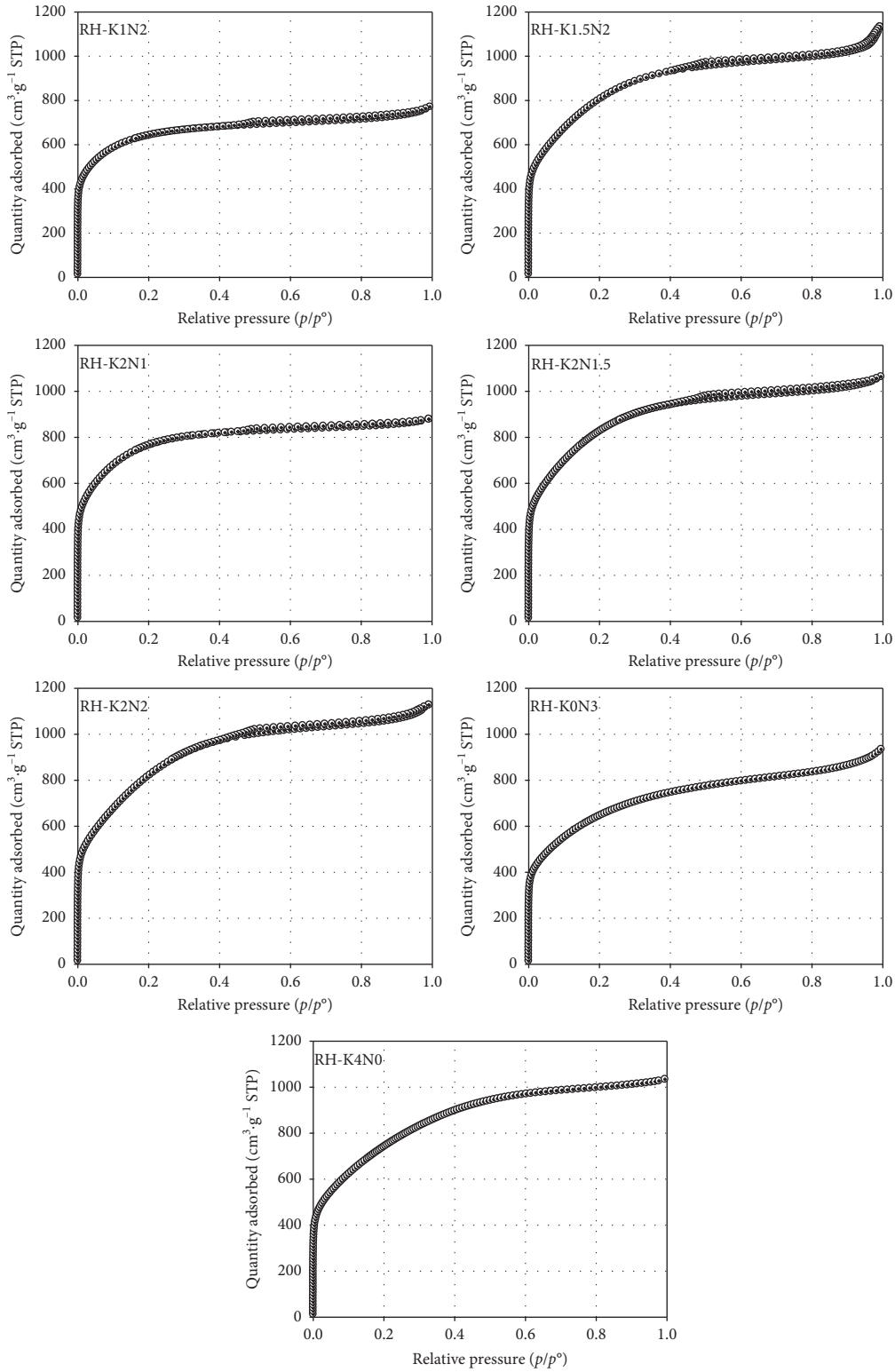

Figure 1: Adsorption-desorption isotherms of N_2 at 77K for AC samples (the same scale on the quantity adsorbed axes was maintained to enable better comparison between graphs).

Figure 2 shows the pore-size distributions (PSDs) calculated from the N_2 adsorption isotherm by applying the DFT method. It can be noticed that a considerable amount of pores is distributed in the range from 0.8 to 1.8 nm, and from 1.8 to 5 nm, further indicating the concurrence of micropores and mesopores, which corresponds well with the observation from N_2 adsorption/desorption at 77K in Figure 1. Combined with the summarized data in Table 1, it

Table 2: Physical properties deduced from N_2 adsorption at 77K of AC samples.

Sample	S_{BET} ($m^2 \cdot g^{-1}$)	S_{mic} ($m^2 \cdot g^{-1}$)	S_{ext} ($m^2 \cdot g^{-1}$)	V_{mic} ($cm^3 \cdot g^{-1}$)	V_{mes} ($cm^3 \cdot g^{-1}$)	V_{tot} ($cm^3 \cdot g^{-1}$)	V_{mic}/V_{tot} (%)
RH-K4	2696	2470	226	1.4258	0.3111	1.7369	82.1
RH-N3	2360	2065	295	1.0927	0.4396	1.5323	71.3
RH-K1N2	2365	2258	107	1.0156	0.1846	1.2002	84.6
RH-K1.5N2	2945	2745	200	1.3811	0.4200	1.8011	76.7
RH-K2N1	2829	2736	93	1.2267	0.1369	1.3636	90.0
RH-K2N1.5	3043	2831	211	1.4250	0.2962	1.7212	82.8
RH-K2N2	2990	2747	243	1.4316	0.3768	1.8084	79.2

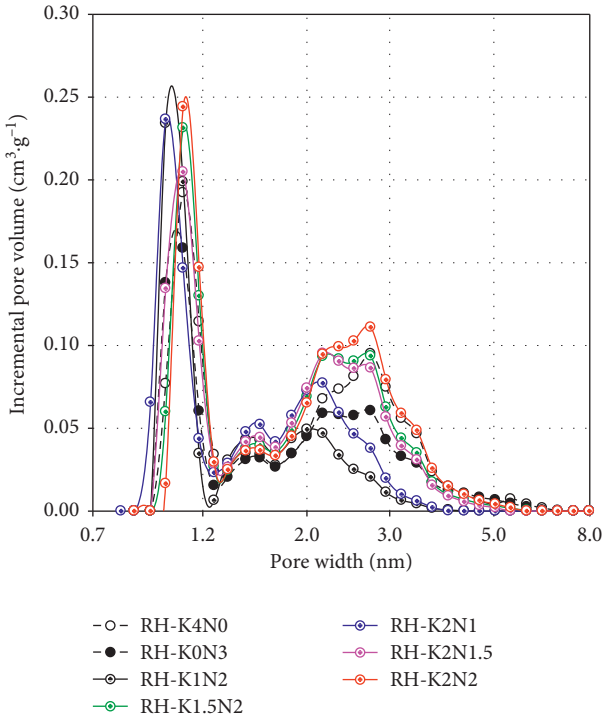

Figure 2: Pore-size distribution of AC samples.

can be seen that the total volume is increasing with the increase of alkali hydroxide/char ratios and V_{tot} is highest with alkali hydroxide/char = 4.0 (RH-K2N2). At the same amount of alkali hydroxide/char, the higher KOH content resulted in the development of microporosity. V_{mi}/V_{tot} of RH-K2N1.5 and RH-K2N1 (82.8% and 90.0%) are higher than those of RH-K1.5N2 and RH-K1N2 (84.6% and 76.7%). According to Alcaniz-Monge and Illan-Gomez [20], the development of microporosity is due to carbon gasification and the metal intercalation, and only KOH generates supermicroporosity.

With the significantly improvement of porous characteristic of activated carbons by employing dual activation agents and by varying the KOH/NaOH ratio, we focus on dual activation agents in further studies.

3.1.2. SEM Analysis. The SEM micrographs of AC samples are shown in Figure 3. All samples exist in the form of spherical-shaped particles with the size ranging from 20 to 60 nm. The impregnation ratios only have slight effect on the compact of the samples. There are more cracks and crevices as the KOH/NaOH ratios increase, and the samples with higher amount of impregnated KOH are more porous than the other.

3.1.3. Element Analysis. The element analysis of AC samples was determined by EDX measurement and is given in Table 3. All the samples have relatively high carbon content (94.38~95.23%) and no or less than 0.09% silica content. This is due to the use of the alkali hydroxide activation agent which reacts with silica (relatively rich in rice husk) to form alkali silicate and be removed in the washing process [21]. The presence of oxygen (4.54~5.35%) is owing to the adsorbed water and surface functional groups. The existence of Cl, Cr, and Fe might be caused by the reactor container during the activation process and by HCl washing thereafter. Neither K nor Na has been detected, which demonstrates the effectiveness of the washing process.

3.1.4. FTIR Analysis. The FTIR spectra of all the AC samples are shown in Figure 4, which have similar shapes with most of the peaks located at the same wave number. The wide bands located at 3450 cm^{-1} can be attributed to the presence of –OH vibration [22]. The band at 2920 and 2860 cm^{-1} may be assigned to the presence of aliphatic C–H vibration [23]. The strong band at 1630 nm represents the C=O vibration [24]. The peak at 1384 cm^{-1} is ascribed to CH_2 and CH_3 groups [23]. There is no SiO_2 absorption peaks (at 1101, 944, and 789 cm^{-1} [25]), indicating that silica has been successfully removed from the samples. The obtained result is consistent with earlier EDX studies, in which Si content of all AC samples is less than 0.1%.

3.1.5. Boehm Titration. The acid/base properties of the AC samples are evaluated by Boehm titration and shown in Table 4. From the results in Table 4, it can be observed that the acidic sites are dominant over basic sites. Total amount of acidic groups is in the range of 1.387~1.771 $mmol \cdot g^{-1}$ whereas the amount of basic groups is only from 0.346 to 0.704 $mmol \cdot g^{-1}$. The smallest amount of total acidic groups is found at the RH-K1.5N2 sample (1.387 $mmol \cdot g^{-1}$) and the highest at the RH-K2N1.5 sample (1.771 $mmol \cdot g^{-1}$). This result is in good agreement with the EDX measurement that oxygen content is lowest and highest in RH-K1.5N2 (4.54%) and

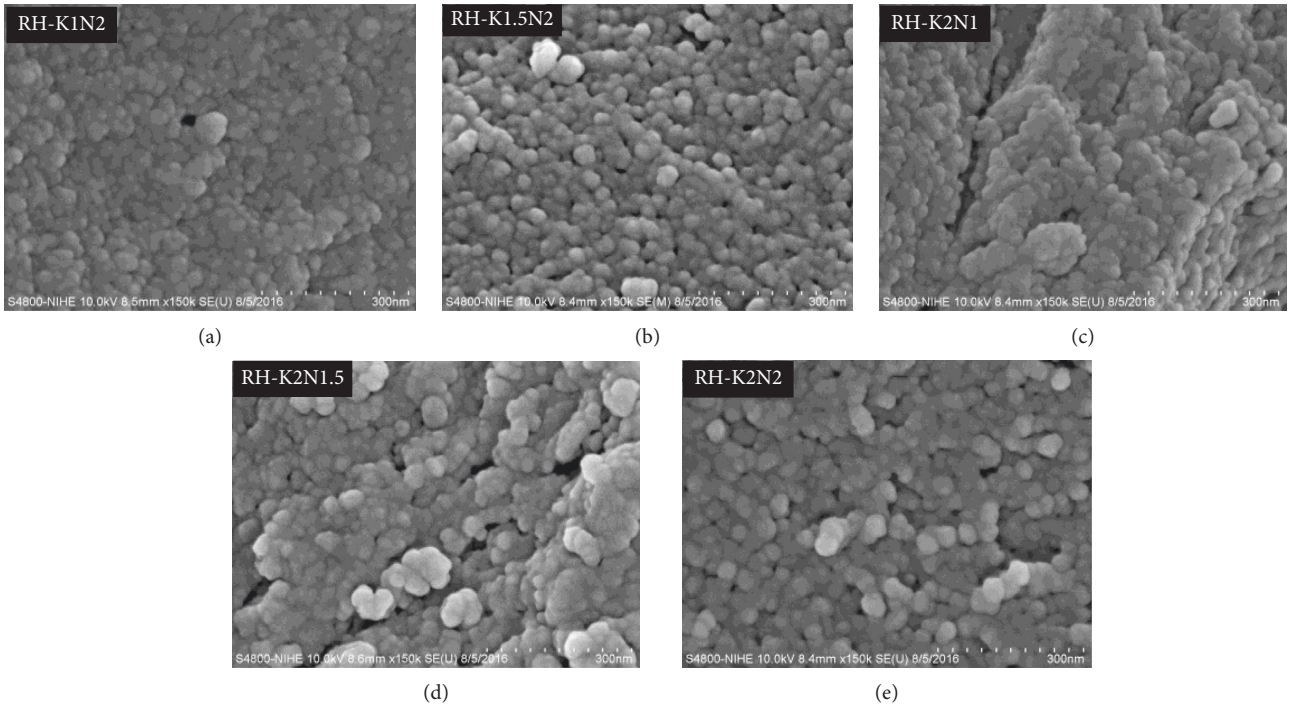

Figure 3: SEM images of AC samples.

Table 3: EDX analysis of AC samples.

Sample	Mass percentage						
	C	O	Si	Cl	Cr	Fe	Total
RH-K1N2	94.67	5.13	0	0.09	0.05	0.06	100
RH-K1.5N2	95.23	4.54	0.08	0.04	0.06	0.05	100
RH-K2N1	94.91	4.92	0.07	—	0.04	0.06	100
RH-K2N1.5	94.38	5.35	0.09	0.08	0.05	0.05	100
RH-K2N2	94.79	5.09	—	—	0.06	0.06	100

in RH-K2N1.5 (5.35%), respectively. It can also be noticed from Table 4 that the numbers of carboxylic, phenolic, and lactonic groups as well as total basic groups are almost unrelated to the amount of alkali hydroxide used or the KOH/NaOH impregnation ratio.

3.1.6. Raman Analysis. The degree of surface disorder and defect of the as-prepared AC samples were evaluated by Raman spectra and are illustrated in Figure 5 and Table 5. There are graphite (G) peak at 1580 cm^{-1} and the defect-disorder (D) peak at 1350 cm^{-1}. The G-peak is associated with E_{2g}, and the D-peak is corresponded to A_{1g}. The ratio of the integrated intensities of D-band and G-band (I_D/I_G) is consistent with the degree of graphitization of carbonaceous materials, and I_D/I_G increases with the decreasing in crystallinity [26]. The results from Table 5 reveal that RH-K2N1.5 has the highest I_D/I_G value which indicates the highest surface disorder degree of this sample. The I_D/I_G values of RH-K1.5N2 and RH-K2N2 are 1.361 and 1.291, suggesting that these two samples have higher degree of graphite organization. This outcome confirms the Boehm titration results, since the surface disorder degree is

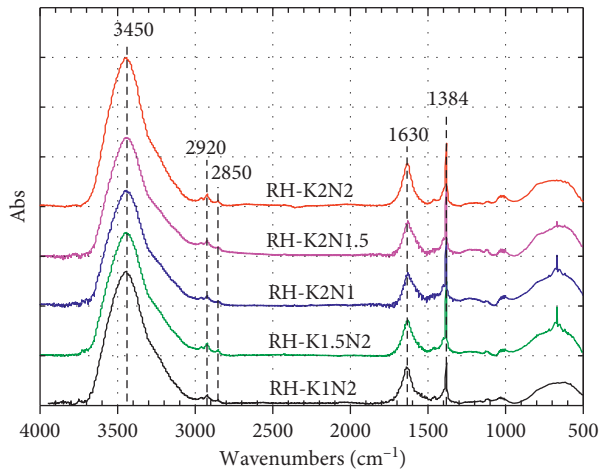

Figure 4: FTIR spectra of AC samples.

resulting from high amount of surface functional groups. The crystalline size along the basal plane (L_a) in Table 5 was calculated by the following equation [27]: $L_a\,(nm) = (4.35 \times I_G)/I_D$ (3). RH-K1.5N2 and RH-K2N2 have low value of I_D/I_G; consequently, their calculated crystallite sizes are towering over other samples.

3.1.7. TGA Analysis. Figure 6 shows the TGA-DTA curves of AC samples prepared at different KOH/NaOH/char ratios. All samples show a similar behavior in the temperature range under study, which occurs in two weight-loss stages: 120~350°C and 350~600°C. The weight loss in the temperature range of 120~350°C is summarized in

Table 4: Functional groups on the surface of AC samples by Boehm titration.

Sample	Functional groups (mmol g^{-1})				
	Carboxylic	Phenolic	Lactonic	Acidic site	Basic site
RH-K1N2	0.500	0.850	0.250	1.600	0.630
RH-K1.5N2	0.495	0.397	0.495	1.387	0.693
RH-K2N1	0.350	0.550	0.600	1.500	0.690
RH-K2N1.5	0.260	0.990	0.521	1.771	0.704
RH-K2N2	0.445	0.595	0.545	1.585	0.346

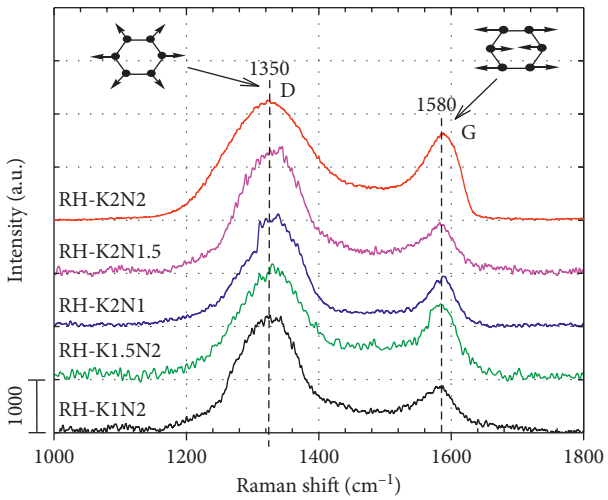

Figure 5: Raman analysis of AC samples.

Table 5: I_D, I_G, I_D/I_G, and L_a.

Sample	I_D (a.u.)	I_G (a.u.)	I_D/I_G	L_a (nm)
RH-K1N2	1875	838	2.237	1.94
RH-K1.5N2	1870	1374	1.361	3.20
RH-K2N1	1889	859	2.199	1.98
RH-K2N1.5	2205	918	2.402	1.81
RH-K2N2	2021	1566	1.291	3.37

Table 6. The weight loss of all the samples in this range is lower than 5.09% and is due to the decomposition of some oxygen containing groups (carboxylic 100–250°C and lactonic 200–400°C [28]). Hence, for the convenience of comparison, the amount of carboxylic and lactonic groups evaluated from Boehm titration is also presented in Table 6. Table 6 shows that there is a consistency between the weight loss and the total amount of carboxylic and lactonic groups, which further confirms the Boehm titration results above.

It also has to be pointed out that the main difference between TGA-DTA curves is only shown in the exothermic peaks of the second weight loss range. At the same impregnated alkali hydroxide amount, the exothermic peak temperature is lower for higher KOH content (between RH-K2N1.5 and RH-K1.5N2 or between RH-K2N1 and RH-K1N2) confirming that KOH is a more reactive agent, in comparison with NaOH [29].

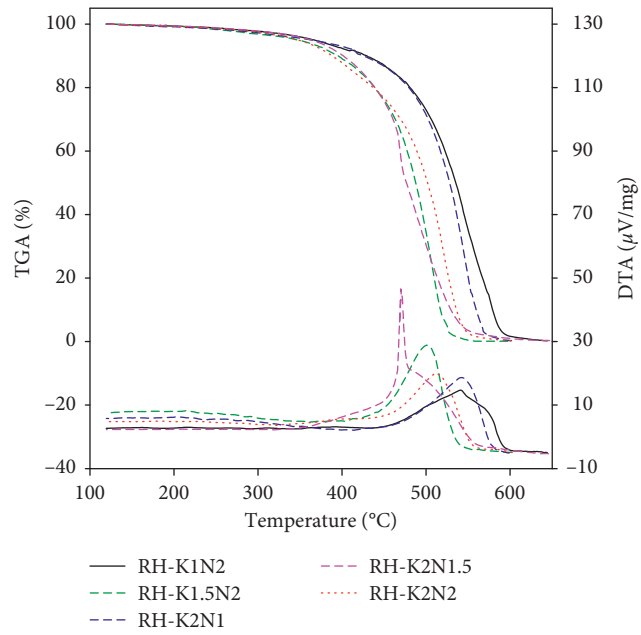

Figure 6: TGA-DTA curves of AC samples.

Table 6: Weight loss of AC samples and total carboxylic and lactonic groups.

Sample	Weight loss (%) in the temperature range of 120~350 (°C)	Total carboxylic and lactonic groups (mmol g^{-1})
RH-K1N2	4.01	0.750
RH-K1.5N2	5.09	0.990
RH-K2N1	4.45	0.950
RH-K2N1.5	4.10	0.781
RH-K2N2	5.02	0.990

3.2. Electrochemical Features. The electrochemical performance of electrodes made of the as-prepared AC samples was evaluated using cyclic voltammetry and galvanostatic charge/discharge. Figure 7 depicts cyclic voltammograms of AC electrodes in 0.5 M K_2SO_4 electrolyte at four typical scan rates 2, 10, 30, and 50 m·V s^{-1} in the potential windows of −1.0~0.0 V vs. SCE. At 2 mV·s^{-1}, CV curves exhibit a symmetric rectangular shape with a slight distortion, indicating an ideal electrochemical double-layer capacitor behavior. The little hump appeared in CV curves of AC electrodes can be accounted for the reaction of surface functional groups [30].

In detail, as the scan was initiated at 0.0 V in negative direction to −1.0 V, the K^+ ions immigrated to the activated carbon surface, diffused into the pores, and adsorbed onto the surface as well as inside the pores to form an electrical double layer. The specific capacitance of activated carbon is caused by the double-layer capacitance of the adsorbed K^+ ions (positive charge) and the electrons accumulated on the carbon surface (negative charge) as well as the pseudocapacitance provided by the reduction of surface functional

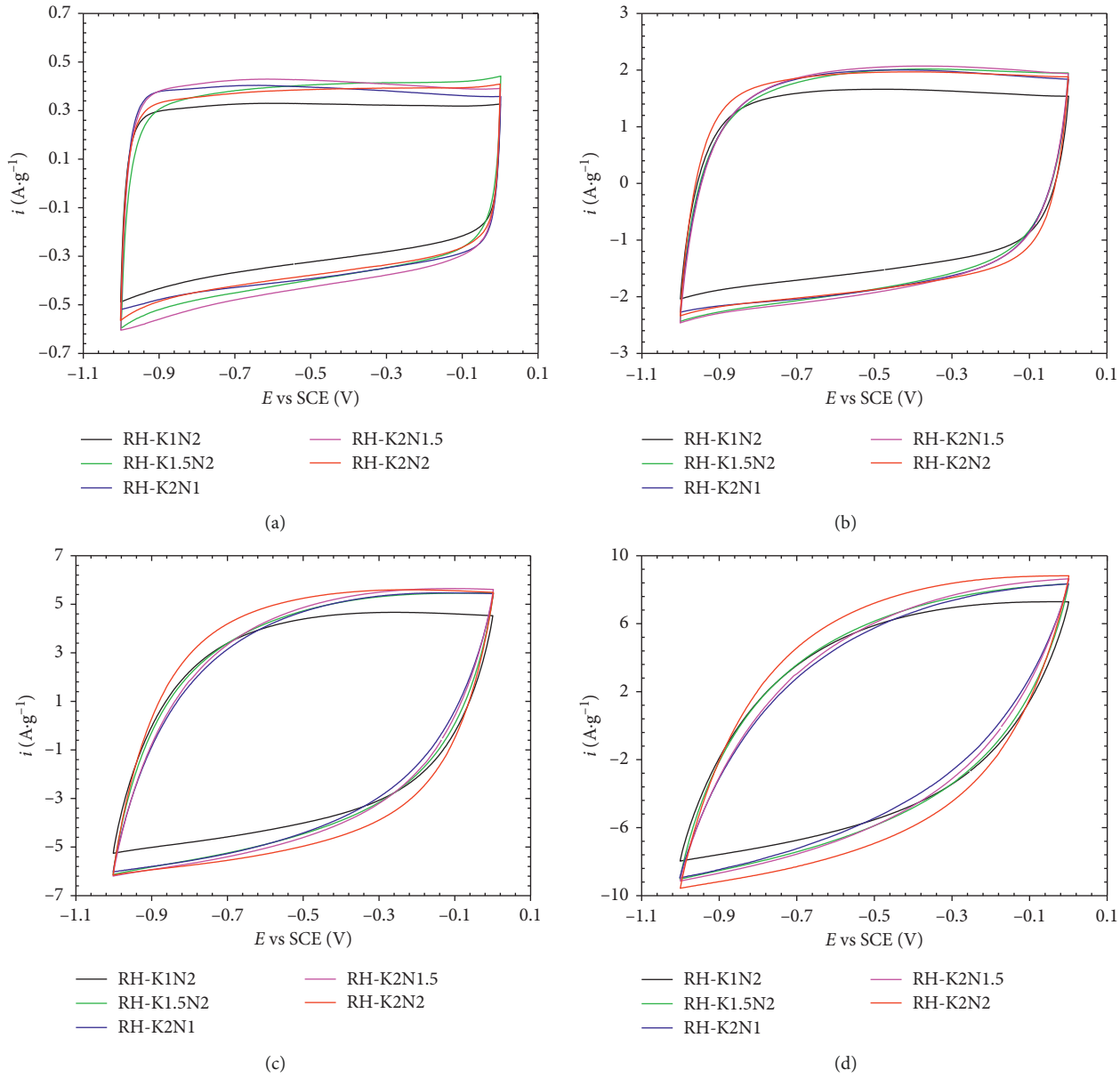

Figure 7: Cyclic voltammograms of AC samples in 0.5 M K_2SO_4 at different scan rates from 2 to 50 mV·s^{-1}. (a) $v = 2$ mV·s^{-1}, (b) $v = 10$ mV·s^{-1}, (c) $v = 30$ mV·s^{-1}, and (d) $v = 50$ mV·s^{-1}.

groups. By reverse scan from −1.0 to 0.0 V, the K^+ ions are desorbed and diffused out of the pores. Simultaneously with this process, there exists the oxidation of surface functional groups. According to Frackowiak and Béguin [31], the redox reaction can be described as follows:

$$\begin{aligned} &>C-OH \rightleftarrows >C=O+H^+ + e \\ &-COOH \rightleftarrows -COO + H^+ + e \\ &>C=O + e \rightleftarrows >C-O^- \end{aligned} \quad (3)$$

As the scan rate increases from 2 to 10, 30, and further to 50 mV·s^{-1}, the CV curves are deformed. The deviations from the rectangular shape are more pronounced with increasing scan rate and in the order RH-K2N2 < RH-K2N1.5 < RH-K1.5N2 < RH-K1N2 < RH-K2N1. This is due to the kinetic limitation of the adsorption/desorption rate of K^+ ions which is directly affected by the diffusion of K^+ ions into and out of the micropores of AC electrodes. This, in turn, will increase the resistance of AC materials, leading to a deformed rectangle [32]. RH-K2N2 has the largest external surface (243 m^2·g^{-1}); thus, it is the least affected by the scan rate. By contrast, as the external surface of RH-K2N1 (93 m^2·g^{-1}) is smallest, its CV curve is the most deviated from the ideal shape.

The specific capacitances calculated from CV curves at different scan rates are summarized in Table 7. All the calculated C_{CV} are in the range of 160~205 F·g^{-1} at the scan rate of 2 mV·s^{-1}. These values are about 1.6~2 times of the

Table 7: C_{CV} at different scan rates.

Sample	C_{CV} (F g^{-1}) at different scan rates						
	2 mV·s^{-1}	5 mV·s^{-1}	10 mV·s^{-1}	20 mV·s^{-1}	30 mV·s^{-1}	50 mV·s^{-1}	100 mV·s^{-1}
RH-K1N2	160	155	147	134	123	103	72
RH-K1.5N2	197	182	167	144	128	111	83
RH-K2N1	191	179	169	149	134	102	69
RH-K2N1.5	205	193	179	157	140	114	74
RH-K2N2	193	184	176	162	149	127	90

PICATIF activated carbon in the same testing conditions [33]. This is owing to the high specific surface area of the as-prepared activated carbons. RH-K2N1.5 and RH-K1N2 has the highest and lowest specific surface area (3043 vs. 2365 $m^2 \cdot g^{-1}$); for that reason, the C_{cv} of RH-K2N1.5 is the highest (205 $F \cdot g^{-1}$) and of RH-K1N2 is the lowest (160 $F \cdot g^{-1}$). Besides, the contribution of surface functional groups should be taken into account, especially at the low scan rate. The highest amount of acidic and basic groups of RH-K2N1.5 (2.475 mmol·g^{-1}) also help raising its specific capacitance.

As the scan rate increases, the specific capacitance of the sample decreases. However, at the scan rate heighten up to 50 mV·s^{-1}, specific capacitances of all samples are still greater than 100 $F \cdot g^{-1}$, which implies the good capacitance of the as-prepared activated carbon in the K_2SO_4 electrolyte. With the increasing scan rate, the specific capacitance decreases gradually, which could be due to the limited diffusion of K^+ ions. At the scan rate as high as 100 mV·s^{-1}, the highest specific capacitance of 90 $F \cdot g^{-1}$ was observed with the RH-K2N2 sample while the lowest of 69 $F \cdot g^{-1}$ was seen in the RH-K2N1 sample. This result might be explained by the effect of the external area of the samples as described above.

Figure 8 displays the charge/discharge curves of AC electrodes at two typical current densities 0.5 and 3.0 $A \cdot g^{-1}$ in 0.5 M K_2SO_4 electrolyte. A good linear variation of potential vs. time is observed for all curves, and the charge curves are symmetric to the corresponding discharge counterparts. There are only small Ohmic drops at high current density, implying the small resistivity of the cell. The Ohmic drops increase with but not proportional to the increasing of current density. At current density of 0.5 $A \cdot g^{-1}$, the Ohmic drops increase in the order RH-K2N2 RH-K1.5N2 < RH-K2N1 RH-K1N2 < RH-K2N1.5. At current density of 3.0 $A \cdot g^{-1}$, however, the order changes to RH-K2N2 < RH-K2N1.5 < RH-K1.5N2 < RH-K1N2 < RH-K2N1.

The difference in the Ohmic drop is owing to the internal resistance of materials, and the less mesopores (lower external surface), the higher the internal resistance. However, the surface disorder of the material also adds up to the increase of internal resistance. The Raman results in Table 5 show that the surface disorder increase in the following order: RH-K2N2 < RH-K1.5N2 < RH-K2N1 < RH-K1N2 < RH-K2N1.5. This means that the surface conductivity of the samples decreases in order RH-K2N2 > RH-K1.5N2 > RH-K2N1 > RH-K1N2 > RH-K2N1.5, which is consistent with the magnitude of Ohmic drops at low current density (0.5 $A \cdot g^{-1}$). At high current density, the Ohmic drop strongly depends on the mesopores amount. RH-K2N2 has the highest mesopores amount (BET result in Table 2); therefore, it has the smallest Ohmic drop. In contrast, the Ohmic drop of RH-K2N1 is highest owing to its low mesopores amount.

The gravimetric specific capacitances at different current densities calculated from equation (2) are illustrated in Figure 9. It can be seen from Figure 9 that the specific capacitance decreases with the increasing of current density. As current density increases from 0.2 to 3.0 $A \cdot g^{-1}$, the specific capacitance of RH-K2N1.5 decreases from 225 to 154 $F \cdot g^{-1}$. It also can be seen from Figure 9 that the change in the specific capacitance of AC samples with current density is similar to the change with the scan rate (described above). This result confirms the CV result and can also be explained due to Raman as well as BET result.

4. Conclusions

High surface area activated carbons from rice husk have been prepared by chemical activation with dual activation agents, KOH and NaOH. The activation condition, namely, total alkali hydroxide/char and KOH/NaOH ratio can affect the pore structure of the activated carbons. The as-prepared activated carbon samples have a porous structure with developed specific surface area (2365~3043 $m^2 \cdot g^{-1}$) and high pore volume (1.2002~1.8084 $cm^3 \cdot g^{-1}$). The alkali hydroxide/char and KOH/NaOH ratio have a significant effect on the pore texture of AC samples. The AC sample prepared with alkali hydroxide/char = 3.0 and KOH/NaOH = 0.5 has specific surface area and pore volume as 2365 $m^2 \cdot g^{-1}$ and 1.2002 $cm^3 \cdot g^{-1}$, respectively. Alkali hydroxide/char = 3.5 and KOH/NaOH = 1.33 give the highest specific surface area of 3043 $m^2 \cdot g^{-1}$ and pore volume of 1.7212 $cm^3 \cdot g^{-1}$. The as-prepared AC samples have particle size in the range of 20~60 nm and were estimated to have more than 94% carbon, about 5% oxygen, and a trace amount of other elements (Si, Cl, Cr, and Fe). The presence of oxygen is due to the adsorbed water and surface functional groups (1.931~2.475 mmol·g^{-1}). All the AC samples exhibit a good capacitive behavior when used as an electrode material of supercapacitors. In the 0.5 M K_2SO_4 electrolyte, the highest capacitance obtained is 205 $F \cdot g^{-1}$ at the scan rate of 2 mV·s^{-1} and is 225 $F \cdot g^{-1}$ at the current density of 0.2 $A \cdot g^{-1}$. This result shows the potential for valorization of rice husk waste by

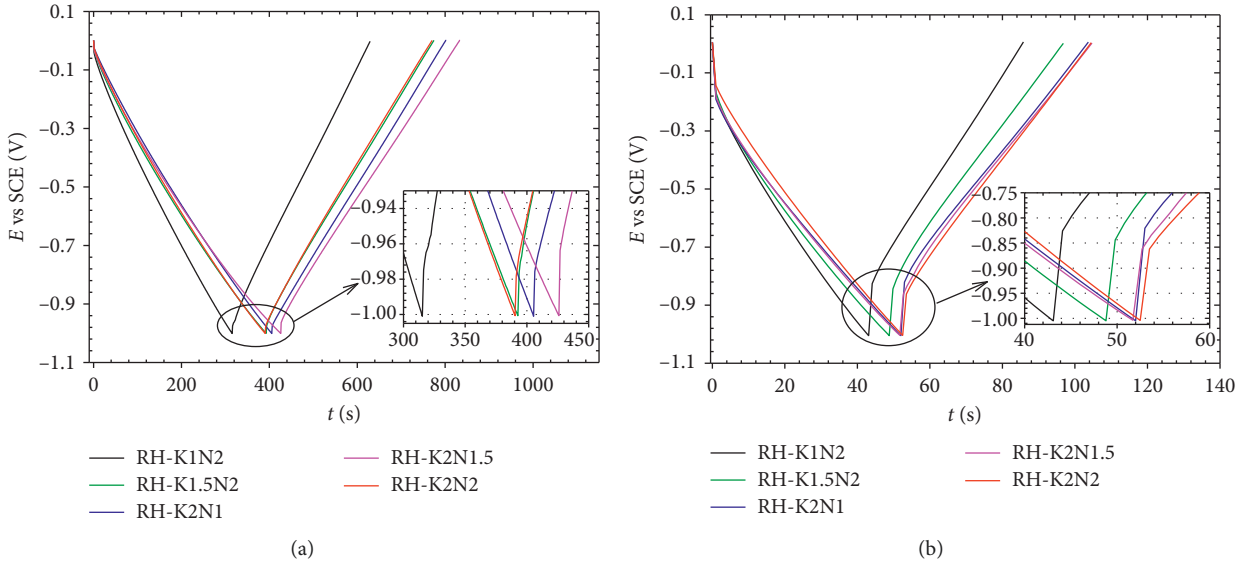

Figure 8: Charge-discharge curves of AC electrode at two different current densities. (a) $i = 0.5\ A{\cdot}g^{-1}$ and (b) $i = 3.0\ A{\cdot}g^{-1}$.

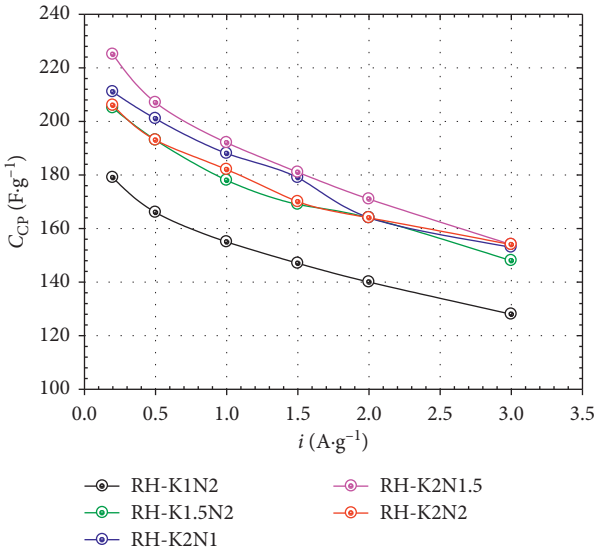

Figure 9: Gravimetric specific capacitances of AC electrodes at different current densities.

controlling the specific surface area and pore structure of the prepared activated carbon toward the application as a supercapacitor electrode.

Data Availability

The datasets used to support the findings of this study are available from the corresponding author upon request.

Conflicts of Interest

The authors declare that there are no conflicts of interest regarding the publication of this paper.

Acknowledgments

This research has received funding from the Vietnamese Ministry of Education and Training under grant number B2016-SPH-20.

References

[1] S. J. Sahira, A. Mandira, P. B. Prasad, and P. R. Ram, "Effects of activating agents on the activated carbons prepared from Lapsi seed," *Research Journal of Chemical Sciences*, vol. 3, no. 5, pp. 19–24, 2013.

[2] A. Ahmadpour, B. A. King, and D. D. Do, "Comparison of equilibria and kinetics of high surface area activated carbon produced from different precursors and by different chemical treatments," *Industrial and Engineering Chemistry Research*, vol. 37, no. 4, pp. 1329–1334, 1998.

[3] Y. Gao, Q. Yue, B. Gao et al., "Comparisons of porous, surface chemistry and adsorption properties of carbon derived from Enteromorpha prolifera activated by $H_4P_2O_7$ and KOH," *Chemical Engineering Journal*, vol. 232, pp. 582–590, 2013.

[4] N. Ozbay and A. S. Yargic, "Comparison of surface and structural properties of carbonaceous materials prepared by chemical activation of tomato paste waste: the effects of activator type and impregnation ratio," *Journal of Applied Chemistry*, vol. 2016, Article ID 8236238, 10 pages, 2016.

[5] R.-L. Tseng, "Mesopore control of high surface area NaOH-activated carbon," *Journal of Colloid and Interface Science*, vol. 303, no. 2, pp. 494–502, 2006.

[6] A. Ahmadpour, H. Rashidi, M. J. D. Mahboub, and M. R. Farmad, "Comparing the performance of KOH with NaOH-activated anthracites in terms of methane storage," *Adsorption Science and Technology*, vol. 31, no. 8, pp. 729–745, 2013.

[7] E. Raymundo-Piñero, P. Azaïs, T. Cacciaguerra, D. Cazorla-Amorós, A. Linares-Solano, and F. Béguin, "KOH and NaOH activation mechanisms of multiwalled carbon nanotubes with

different structural organisation," *Carbon*, vol. 43, no. 4, pp. 786–795, 2005.

[8] K. Le Van and T. T. Luong Thi, "Activated carbon derived from rice husk by NaOH activation and its application in supercapacitor," *Progress in Natural Science: Materials International*, vol. 24, no. 3, pp. 191–198, 2014.

[9] L. Muniandy, F. Adam, A. R. Mohamed, and E.-P. Ng, "The synthesis and characterization of high purity mixed microporous/mesoporous activated carbon from rice husk using chemical activation with NaOH and KOH," *Microporous and Mesoporous Materials*, vol. 197, pp. 316–323, 2014.

[10] S. Brunauer, P. H. Emmett, and E. Teller, "Adsorption of gases in multimolecular layers," *Journal of the American Chemical Society*, vol. 60, pp. 309–319, 1938.

[11] B. Lippens and J. H. de Boer, "Studies on pore systems in catalysts V. The t method," *Journal of Catalysis*, vol. 4, no. 3, pp. 319–323, 1965.

[12] E. P. Barrett, L. G. Joyner, and P. P. Halenda, "The determination of pore volume and area distributions in porous substances. I. Computations from nitrogen isotherms," *Journal of the American Chemical Society*, vol. 73, pp. 373–380, 1951.

[13] P. A. Webb and C. Orr, *Analytical Methods in Fine Particle Technology*, Micromeritics Instrument Corporation, Norcross, GA, USA, 1997.

[14] N. Rambabu, R. Azargohar, A. K. Dalai, and J. Adjaye, "Evaluation and comparison of enrichment efficiency of physical/chemical activations and functionalized activated carbons derived from fluid petroleum coke for environmental applications," *Fuel Processing Technology*, vol. 106, pp. 501–510, 2013.

[15] K. S. W. Sing, D. H. Everett, R. A. W. Haul et al., "Reporting physisorption data for gas/solid systems with special reference to the determination of surface area and porosity (Recommendations 1984)," *Pure and Applied Chemistry*, vol. 57, no. 4, pp. 603–619, 1985.

[16] H. Marsh and F. R. Reinoso, *Activated Carbon*, Elsevier, Amsterdam, Netherlands, 2006.

[17] A. Sirimuangjinda, K. Hemra, D. Atong, and C. Pechyen, "Comparison on pore development of activated carbon produced from scrap tire by potassium hydroxide and sodium hydroxide for active packaging materials," *Key Engineering Materials*, vol. 545, pp. 129–133, 2013.

[18] M. A. Lillo-Ródenas, D. Cazorla-Amorós, and A. Linares-Solano, "Understanding chemical reactions between carbons and NaOH and KOH," *Carbon*, vol. 41, no. 2, pp. 267–275, 2003.

[19] A. Linares-Solano, M. A. Lillo-Rodenas, J. P. Marco-Lozar, M. Kunowsky, and A. J. Romero-Anaya, "NaOH and KOH for preparing activated carbons used in energy and environmental application," *International Journal of Energy, Environment and Economics*, vol. 20, no. 4, pp. 59–91, 2012.

[20] J. Alcañiz-Monge and M. J. Illán-Gómez, "Insight into hydroxides-activated coals: chemical or physical activation?," *Journal of Colloid and Interface Science*, vol. 318, no. 1, pp. 35–41, 2008.

[21] Y. Guo, J. Qi, Y. Jiang, S. Yang, Z. Wang, and H. Xu, "Performance of electrical double layer capacitors with porous carbons derived from rice husk," *Materials Chemistry and Physics*, vol. 80, no. 3, pp. 704–709, 2003.

[22] S. Valizadeh, H. Younesi, and N. Bahramifar, "Highly mesoporous K_2CO_3 and KOH/activated carbon for SDBS removal from water samples: batch and fixed-bed column adsorption process," *Environmental Nanotechnology, Monitoring and Management*, vol. 6, pp. 1–13, 2016.

[23] A. Reffas, V. Bernardet, B. David et al., "Carbon prepared from coffee grounds by H_3PO_4 activation: characterization and adsorption of methylene blue and Nylosan Red N-2RBL," *Journal of Hazardous Materials*, vol. 175, no. 1-3, pp. 779–788, 2010.

[24] A. R. S. Neto, M. A. M. Araujo, F. V. D. Souza, L. H. C. Mattoso, and J. M. Marconcini, "Characterization and comparative evaluation of thermal, structural, chemical, mechanical and morphological properties of six pineapple leaf fiber varieties for use in composites," *Industrial Crops and Products*, vol. 43, pp. 529–537, 2013.

[25] D. An, Y. Guo, B. Zou, Y. Zhu, and Z. Wang, "A study on the consecutive preparation of silica powders and active carbon from rice husk ash," *Biomass and Bioenergy*, vol. 35, no. 3, pp. 1227–1234, 2011.

[26] M. A. Amaral Junior, J. T. Matsushima, M. C. Rezende, E. S. Gonçalves, J. S. Marcuzzo, and M. R. Baldan, "Production and characterization of activated carbon fiber from textile PAN fiber," *Journal of Aerospace Technology and Management*, vol. 9, no. 4, pp. 423–430, 2017.

[27] F. Tuinstra and J. L. Koenig, "Raman spectrum of graphite," *Journal of Chemical Physics*, vol. 53, no. 3, pp. 1126–1130, 1970.

[28] J. L. Figueiredo, M. F. R. Pereira, M. M. A. Freitas, and J. J. M. Órfão, "Modification of the surface chemistry of activated carbons," *Carbon*, vol. 37, no. 9, pp. 1379–1389, 1999.

[29] M. Lillorodenas, J. Juan-Juan, D. Cazorla-Amoros, and A. Linares-Solano, "About reactions occurring during chemical activation with hydroxides," *Carbon*, vol. 42, no. 7, pp. 1371–1375, 2004.

[30] M. Zhang, Y. Li, H. Si, B. Wang, and T. Song, "Preparation and electrochemical performance of coconut shell activated carbon produced by the H_3PO_4 activation with rapid cooling method," *International Journal of Electrochemical Science*, vol. 12, pp. 7844–7852, 2017.

[31] E. Frackowiak and F. Béguin, "Carbon materials for the electrochemical storage of energy in capacitors," *Carbon*, vol. 39, no. 6, pp. 937–950, 2001.

[32] S. Sarangapani, B. V. Tilak, and C.-P. Chen, "Materials for electrochemical capacitors," *Journal of The Electrochemical Society*, vol. 143, no. 11, pp. 3791–3799, 1996.

[33] T. Brouse, P.-L. Taberna, O. Crosnier et al., "Long-term cycling behavior of asymmetric activated carbon/MnO_2 aqueous electrochemical supercapacitor," *J. Power Sources*, vol. 173, no. 1, pp. 633–641, 2007.

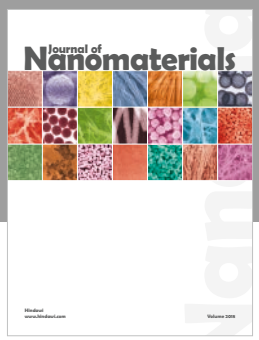

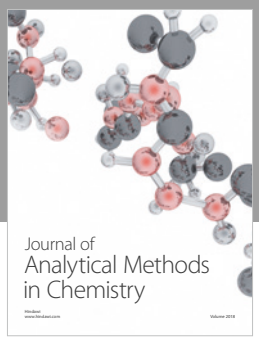

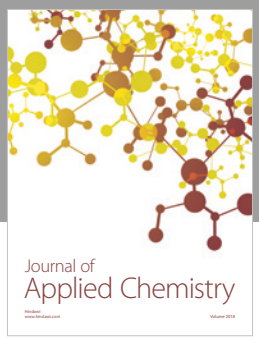

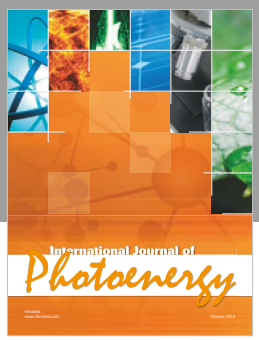

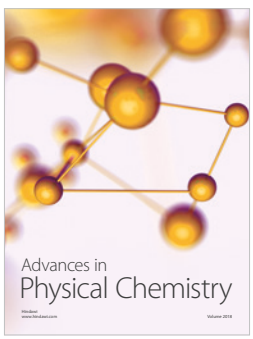

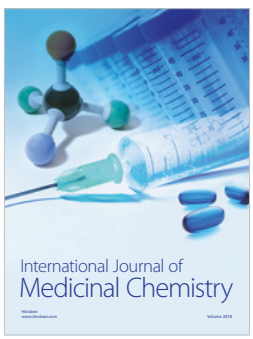

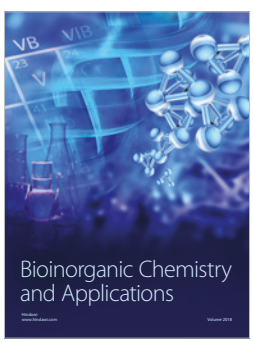

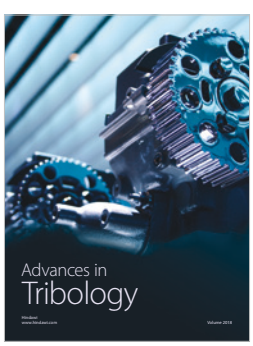

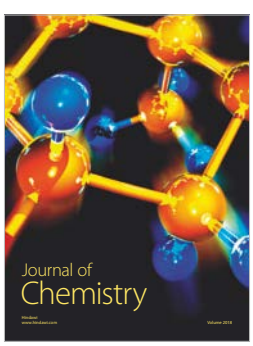

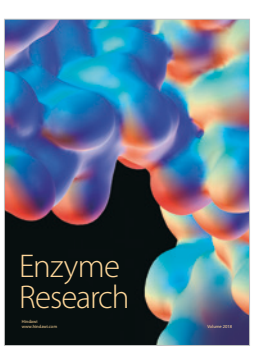

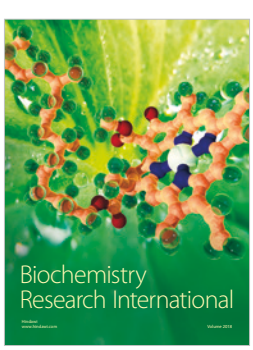

Hindawi

Submit your manuscripts at
www.hindawi.com